Mon. Not. R. Astron. Soc. **000**, 000–000 (0000) Printed 24 April 2003 (MN LATEX style file v2.2)

The X-ray Spectrum of the North Polar Spur

R. Willingale[1], A.D.P. Hands[1], R.S. Warwick[1], S.L. Snowden[2] and D.N. Burrows[3]
[1] *Department of Physics and Astronomy, University of Leicester, University Road, Leicester LE1 7RH*
[2] *Universities Space Research Association, Code 662, NASA GSFC LHEA, Greenbelt, MD 20771, USA*
[3] *Department of Astronomy and Astrophysics, Pennsylvania State University, 525 Davey Lab, University Park, PA 16802, USA*

ABSTRACT
An analysis is presented of the soft X-ray background spectrum measured by the EPIC MOS cameras on *XMM-Newton* in three observations targeted on the North Polar Spur (NPS). Three distinct Galactic plasma components are identified, a cool Local Hot Bubble (LHB) component, $T_{lo} \sim 0.1$ keV, a cool Galactic Halo component at a similar temperature and a hotter component, $T_{hi} \sim 0.26$ keV, associated with the NPS itself. Using the new data in combination with the Rosat All-Sky Survey count rates measured in the 0.1–0.4 keV band, we estimate the emission measure of the LHB material to be 0.0040-0.0052 cm^{-6} pc, which implies an electron density of 0.008-0.011 cm^{-3} and pressure of ~ 22000 cm^{-3} K. The halo and NPS components lie behind at least 50% of the line-of-sight cold gas for which the total Galactic column density is in the range $(2-8) \times 10^{20}$ cm^{-2}. Modelling the X-ray emitting superbubble as a sphere at distance 210 pc, radius 140 pc and centre $l_{II} = 352°$, $b_{II} = 15°$, the implied electron density in the NPS is ~ 0.03 cm^{-3} with pressure ~ 150000 cm^{-3} K. The observed spectral line complexes from OVII, OVIII, FeXVII, NeIX, NeX and Mg XI provide constraints on the composition of the plasma. The hot component in the NPS is depleted in oxygen, neon and, to some extent, magnesium and iron. Assuming the effective line of sight across the halo emission is 1 kpc, the electron density in the halo is 0.007-0.011 cm^{-3} and the pressure is ~ 16500 cm^{-3} K, conditions very similar to those in the LHB.

Key words: ISM:structure - ISM:bubbles - X-rays:interstellar

1 INTRODUCTION

The diffuse Soft X-ray Background (SXRB) originates in a complex blend of Galactic and extragalactic emission components modified by line-of-sight absorption. The *ROSAT* All-Sky Survey (RASS) has provided excellent maps of the SXRB (Snowden et al. 1995, 1997) with a spatial resolution of ~ 12 arc minutes and spectral softness/hardness information based on relatively broad energy bands: 1/4 keV (0.1–0.4 keV), 3/4 keV (0.5–0.9 keV) and 1.5 keV (0.9–2.0 keV). Prominent Galactic features in the 3/4 keV map are the North Polar Spur (NPS), which is part of the radio Loop I emission, and the Galactic Bulge which is evident within $\sim 20°$ of the Galactic Centre, see Fig. 1. The spatial distribution of these features suggests that the emission is truly diffuse and, in fact, there is no known population of low luminosity discrete sources which could account for the observed X-ray flux. The emission is undoubtedly coming from large volumes of hot interstellar gas, perhaps in the form of bubbles, but the detailed 3-D morphology, the origin of the gas, its heating mechanism and its physical state and composition are largely unknown.

The NPS and the rest of Loop I may be a nearby supernova remnant (Berkhuijen et al. 1971) or may have been created by stellar winds from the Sco-Cen OB association, which lies at a distance of 170 pc (Egger & Aschenbach 1995). Equally plausible is the possibility that the observed structures originate due to a combination of these two process. More speculatively they could be part of a bipolar hypershell originating from starburst activity in the Galactic centre ~ 15 million years ago, (Sofue 2000). It is clear that there is significant emission in the direction of Loop I in front of the Ophiuchus Dark Clouds at ~ 150 pc (Snowden et al. 1997), which is not seen in the foreground in other directions (Kuntz & Snowden 1997), supporting a local origin for Loop I. However, emission associated with the Galactic bulge (Snowden et al. 1997) confuses the issue, particularly in the broad region to the north of the Galactic Centre. However, the Galactic bulge emission, if similar in extent in the north as in the south, has a relatively low surface brightness at the longitude and latitude of the NPS.

Spectral measurements with higher resolution are required to discriminate between components of the SXRB and provide reliable physical parameters like temperature and composition for the plasma. Some moderate spectral resolution measurements, mapping at angular scales $> 1°$,

Table 1. Summary of the NPS observations. The N_H is the Galactic value estimated from 21 cm radio observations. The last column indicates the area of diffuse sky visible after removal of point sources with the figures in parentheses representing the sky area after applying a weighting based on the normalised vignetting of the mirrors.

Field	l2°	b2°	N_H cm^{-2}	MOS ksec	arcmin^2
IV NPS	25.0	20.0	8.0×10^{20}	14.1+13.9	576(312)
V NPS	20.0	30.0	5.5×10^{20}	13.1+12.9	586(321)
VI NPS	20.0	40.0	4.0×10^{20}	14.2+14.2	580(318)

indicate a wide range of spectral signatures (Rocchia et al. 1984; Jahoda et al. 1992; Sanders et al. 1993; Gendreau et al. 1995; Mendenhall & Burrows 2001; Sanders et al., 2001; McCammon et al. 2002). In fact most of the available data were recorded in sounding rocket observations with very large fields of view (10's of square degrees) and limited exposure times (typically a few minutes). In contrast the available *ASCA* observations have a small field of view but must be averaged over many different directions to achieve useful statistics (as well as having limited usefulness below ~ 0.7 keV). There is clear evidence that the X-ray spectra of the NPS and Bulge are different, see for example Sanders et al. (1993), but the underlying reasons for such differences are not understood.

2 OBSERVATIONS

The data used here were obtained from the *XMM* EPIC-MOS cameras. These provide a large collecting area of $\sim 1000 \times 2$ cm^2 in the SXRB energy band 0.2–2.0 keV over a circular field of view of 30 arc minutes diameter, combined with moderate angular resolution ($\sim$ 15 arc seconds Half Energy Width). A sequence of six pointings were chosen in regions of high SXRB surface brightness, which were free from known bright X-ray sources. Unfortunately, the first two pointings were badly compromised by bright solar flares and the third missed the intended target, but the remaining three observations yielded a total useful exposure of 84 ksec, roughly 14 ks per field per MOS camera. Fig. 1 shows the three field positions superimposed on the RASS SXRB maps of the Galactic Centre region. The three fields (designated IV, V and VI) lie along the brighter parts of the NPS. Statistics for the three NPS fields are summarised in Table 1.

The EPIC-PN camera was also active during these observations. We have not analysed the PN data for two reasons. Firstly, we have not yet developed a suitable algorithm to extract the diffuse sky background spectrum from the PN data with sufficient sensitivity/reliability and, secondly, the spectral resolution of the PN camera is not as good as the MOS in the 0.5–0.8 keV energy band, which contains the all-important oxygen lines. Eventually inclusion of PN data in the analysis of the SXRB will be important and provide increased sensitivity especially at energies > 1 keV.

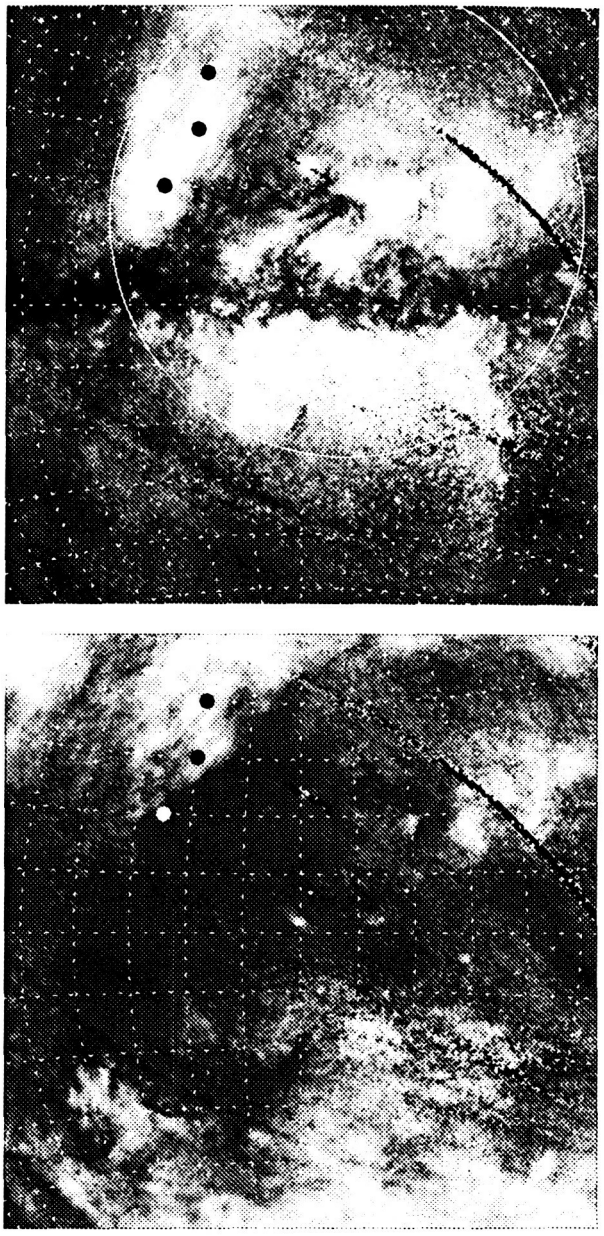

Figure 1. The RASS 0.4–1.2 keV image (top) and 0.1–0.4 keV image (bottom) of the central region of our Galaxy encompassing Loop I and the Galactic Bulge. The small circles show the three pointings along the NPS. The large circle in the upper panel shows the position of the spherical superbubble used for modelling the geometry of the emission. The angular projection is azimuthal equal-area (Lambert) and the grid shows 10 degree squares in Galactic coordinates.

3 FULL-FIELD SPECTRAL EXTRACTION

We have developed an algorithm to extract the diffuse SXRB spectrum from EPIC-MOS data in a robust and reliable way. The basic methodology is similar to that described by Lumb et al. (2002). The major stages in the process are as follows. (i) Initial scanning of the full-field count rate as a function of time to mask out high instrumental background intervals. This must be fairly rigorous because even small excursions above the quiescent level can contaminate the spectrum such that background subtraction is unreliable. (ii) The events

are then sorted into maps with a pixel size of 4 arc seconds and these maps are subjected to a point source search. This is effected by first cross-correlating the map with a circular beam of radius 4 pixels (16 arc seconds), subtracting a smooth background map and then searching for peaks in the resulting image. We require a minimum of 10 net counts per beam and a > 5 sigma fluctuation above the local diffuse background level for a positive detection. The limiting sensitivity to point sources is $\sim 3.3 \times 10^{-15}$ ergs cm^{-2} s^{-1} absorbed (or $\sim 4.2 \times 10^{-15}$ ergs cm^{-2} s^{-1} unabsorbed), 0.4-6.0 keV, in observations of $\sim$ 14 ks, averaged across the field of view of the MOS. (iii) The active sky area of the field of view is defined by the vignetting function. Only regions with an exposure > 25% of the maximum, on-axis, value are included. A significant area of the outer corners of the MOS detectors are masked by the filter housing. These corners still detect particle background and satellite X-ray fluorescence radiation but do not see the diffuse photon flux from the sky. Events within the active sky area are sorted into a pulse height spectrum. The effective response of the instrument over the active sky area is represented by a so-called Auxillary Response File (ARF), which provides the correct weighting of collecting area as a function of energy and position in the field of view. Table 1 lists, for each pointing, the area of sky in the field of view after the exclusion of point sources (in square arc minutes). (iv) The pulse height spectrum produced by the procedure above is contaminated by both the particle and X-ray fluorescence background. We can estimate this background using the masked area of the detectors. In order to get good statistics we accumulated background flux from a number of available pointings (7 Galactic Plane Scan fields, 2 Galactic Ridge fields, 1 Deep Survey field and 4 NPS/Bulge fields) to give a total of 355 ksec of exposure. For all of these data we applied the same rigorous time selection described in (i) above.

Fig. 2 shows a comparison of the SXRB EPIC-MOS count rates (one MOS camera) in the 0.4–1.4 keV band, extracted by the procedure outlined above with the corresponding RASS rates measured in the 0.47–1.21 keV band. The correlation is excellent indicating that the extraction procedures used for the *ROSAT* PSPC and the *XMM* EPIC-MOS are consistent. The residual scatter may well be due to real spectral differences between the fields (when coupled to the very different spectral response of the PSPC and MOS detectors). The expected correlation slope assuming a typical single component thermal SXRB spectrum is 2.4 (MOS rate for one camera) per RASS rate whereas the measured correlation plotted in Fig. 2 is 2.6. The value is dependent on the assumed spectrum and the slightly higher ratio measured is probably due to the small but significant power law component present in the spectrum.

The continuum distribution of the accumulated instrument background was found to be very stable for energies > 0.3 keV. However the bright fluorescence lines from Al K, Si K and Au M lines in the energy range 1.4–2.4 keV do vary with time (and also spatially across the detectors; Lumb et al. 2002). We therefore fit the background continuum with a simple polynomial model masking out these bright lines. The background model is shown in Fig. 3. The fluorescence lines > 5 keV were included in the model since these lines are weak and we have no evidence that they vary significantly with time or over the field of view. We assume that

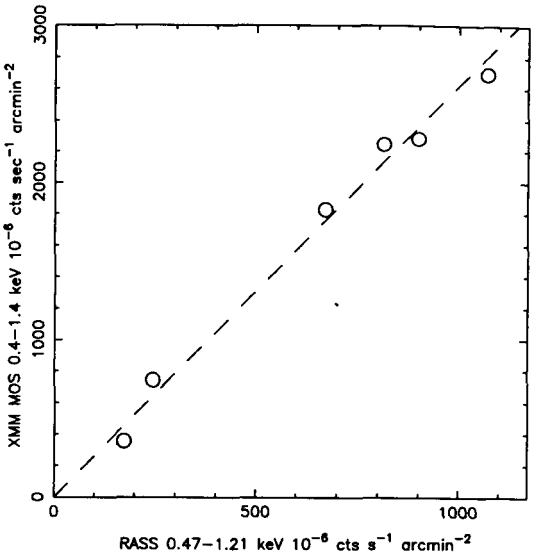

Figure 2. The correlation of the SXRB surface brightness measured in the EPIC-MOS fields in the 0.4–1.4 keV band (count rate in one MOS camera) versus that measured in the RASS between 0.47–1.21 keV. Additional points from a high latitude field, a Galactic Ridge field and a Galactic Bulge field are included to provide coverage of the lower count rate regime.

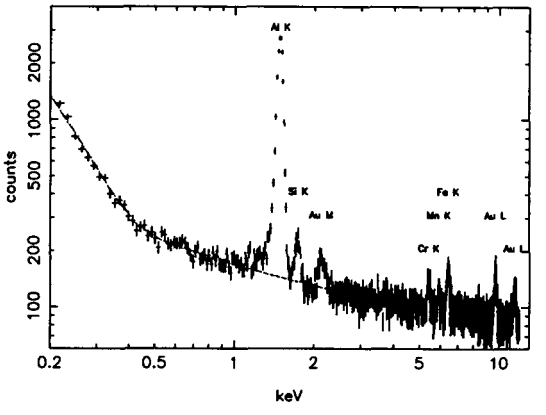

Figure 3. Particle and fluorescent X-ray background accumulated from the masked areas of the MOS detectors in a total exposure time of 355 ksec. The model of the continuum and the fluorescence lines > 5 keV is shown as a smooth curve. The bright AL K, Si K and Au M lines are variable and are not included in the background model.

the resulting modelled background spectrum can be used after scaling as the effective background for the full active field of view. We use as the scale factor the ratio of the count rate measured in the active field region in the 10–11 keV band (which is a spectral region devoid of instrumental fluorescence features and which suffers negligible contamination by hard photons from the cosmic X-ray background) to that similarly measured in the background model. Since the bright fluorescence lines are not included in the background model, the energy range 1.4–2.4 keV must either be excluded from spectral fitting or, alternatively, three extra lines must be included in the spectral model to account for the instrumental Al K, Si K and Au M emission.

4 SPECTRAL ANALYSIS

The measured spectra of the diffuse SXRB were investigated using the XSPEC spectral analysis software package. We utilised the MOS energy band 0.4–1.4 keV, a spectral regime in which there is a significant flux from the SXRB and for which the background subtraction is reliable. A standard MOS spectral binning of 15 eV was used for analysis. The background subtraction was based on the internal instrument background model described above.

We expect a contribution to the SXRB signal below $\sim$ 0.6 keV to come from very soft emission attributable to the Local Hot Bubble (LHB). This component, which is effectively unabsorbed, is particularly strong in the 1/4 keV PSPC band. In order to obtain a reliable estimate of the impact of this local very soft emission on the *XMM-Newton* measurements we carried out joint spectral fits of the MOS spectra with the corresponding RASS 0.1–0.4 keV band count rates (taking into account the appropriate pointing direction and field-of-view scaling factors - see Table 1).[1]

The full spectral model consists of four emission components, three of which are thermal in nature, representing the emission from hot plasmas within our galaxy. The fourth is a non-thermal power-law continuum which we use to represent the extragalactic cosmic X-ray background signal (see Lumb et al. 2002). We model the thermal components in XSPEC using APEC (the Astrophysical Plasma Emission Code) which is the successor to the Raymond & Smith plasma code.

The first thermal component at a temperature T_{lo} ($\sim$ 0.1 keV) is used to represent soft emission from the LHB and is assumed to be completely unabsorbed. The second thermal plasma component is used to model Galactic Halo (GH) emission. On the basis of ROSAT results (Snowden et al. 1997), we set the temperature of this plasma to be the same as that of the LHB (i.e., T_{lo}). However, in the GH case the emission is subject to absorption due to the full interstellar hydrogen column density (see Table 1). Because of the effects of Galactic absorption, the bulk of the observed flux from the GH falls in the 0.4–0.6 keV band, with the OV II emission line being a particularly prominent feature. Interestingly, the EPIC MOS is more sensitive than the ROSAT PSPC in this spectral range because of the prominent carbon absorption edge in the counter window material. The third thermal component has a higher temperature, T_{hi} ($\sim$ 0.3 keV) and dominates the observed spectra at 0.75 keV. We use this component to model emission from the NPS itself and include some fraction of the total Galactic interstellar column density as foreground absorption on this component. In modelling the extragalactic background we assume a broken power-law continuum with a photon index $\gamma = 2.0$ below 0.7 keV and $\gamma = 1.4$ above. This continuum is subjected to the full Galactic absorption. The increase in photon index below 0.7 keV represents the contribution to the background of the QSO population which has been resolved at faint fluxes by ROSAT and Chandra. The normalisation of the power-law for each pointing was derived from the observed 2–10 keV flux but was found to be in good agreement with the results of Lumb et al. (2002). An Al-K emission line is included in the spectral model to fit the prominent fluorescence line which was not included in the background model. We need include only this line since the Si K and Au M fluorescence lines discussed above lie outside of the 0.1-1.4 keV bandpass.

Spectra from the three fields were fitted simultaneously. In an initial trial assuming solar metal abundances, the T_{lo} and T_{hi} parameters were allow to take different values from field to field (i.e., were "untied"). However, the derived T_{lo} values were in each case close to 0.1 keV and hence we fixed T_{lo} at this value for all three fields in the subsequent analysis. Since the T_{hi} values showed small differences between the fields (in the range 0.24-0.28 keV), possibly reflecting variations in the the NPS itself, this parameter was kept "untied".

Finally, in order to get an acceptable fit to several of the prominent lines in the MOS data we found that it was necessary to allow the abundances of O, Ne, Fe and Mg in the high-temperature plasma to deviate from the solar norm. Initially these metal abundances were fitted separately for each individual field. However, since the three fields gave similar results, the abundance for each element was tied in the joint fit.

Fig. 4 shows the best-fit folded model spectra compared with the observed count spectrum for each of the three fields. The hot NPS component dominates down to 0.4 keV in all three fields and all the way down to 0.1 keV for Field VI. The unabsorbed low-temperature component is a significant fraction of the flux in the two RASS bands for all the fields and is the largest contributer in Field IV. The absorbed low-temperature component provides the bulk of the O VII emission and other unresolved low-energy lines but nothing at O VIII, whereas the high-temperature component produces all of the O VIII, Fe XVII, Ne IX and Mg XI emission. It is evident from Fig. 4 that the extragalactic power-law continuum is a relatively insignificant component in the spectral regime of primary interest (0.4-1.4 keV) due to the fact that we have selected very bright regions of the NPS for study.

5 COMPONENTS OF THE ISM IN THE DIRECTION OF THE NPS

The use of a two-temperature model with $T_{lo} \approx 10^6$ K and $T_{hi} \approx 10^{6.4}$ K is, at first sight, fully consistent with the recent *ROSAT* results of Kuntz & Snowden (2001; hereafter KS). However, the KS analysis considers the "typical" high latitude sky, whereas here we are specifically concerned with the bright emission of the NPS. If we presume that the hotter KS component is widespread in the Galaxy then the implication is that our hot NPS component may well include a contribution from this quarter. However, the NPS in the region of our observations is a factor of five or so brighter that the typical high-latitude background in the 0.4 - 1.4 keV band and so hereafter we ignore this complication. On this basis, the combination of RASS and MOS spectra considered here clearly identifies three components of the ISM in the direction of the NPS, namely the LHB, the NPS emission and a soft GH component.

Recently Hutchinson, Warwick & Willingale (2003, her-

[1] We also performed fits including the higher energy RASS bands. However, as these gave essentially the same results, albeit with a slightly higher chi-squared values, in this paper we focus solely on the MOS+RASS(0.1–0.4 keV) joint fits.

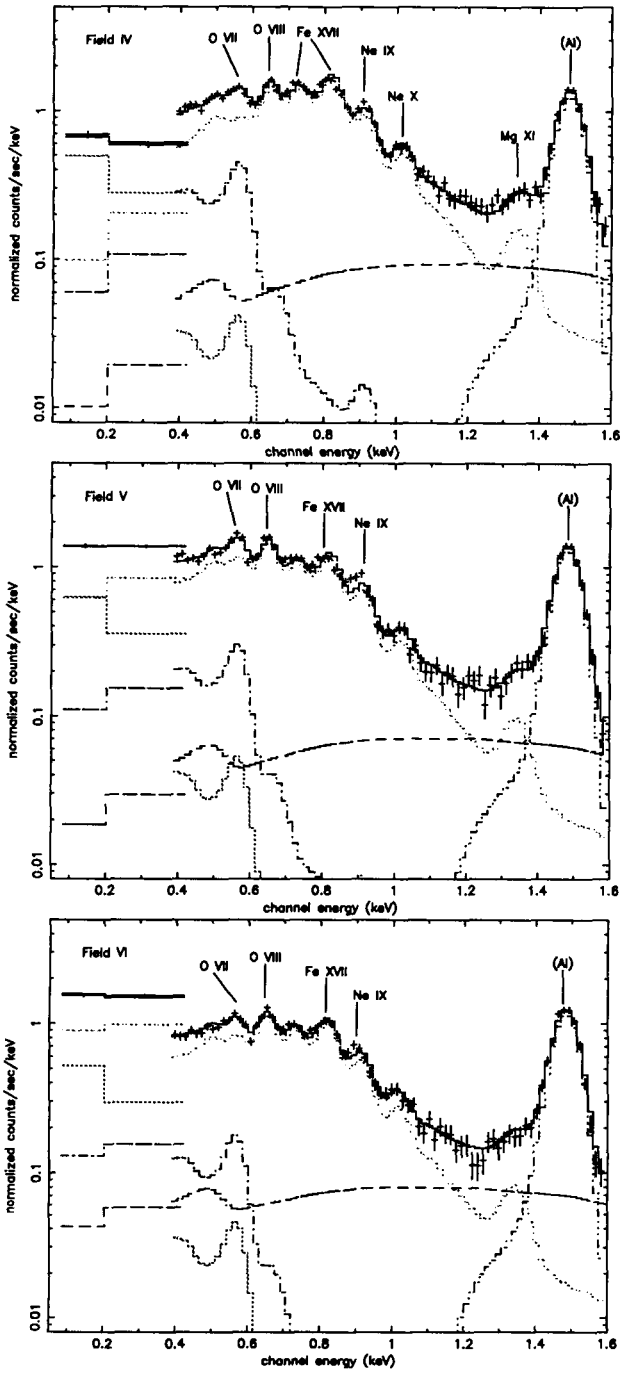

Figure 4. The observed SXRB count spectra compared with the best-fit model. Prominent line complexes are indicated. The 0.1–0.4 keV RASS count rates (bands R1 and R2) are represented by the two broad bins on the left of the plot. The contributions from the four emission components are shown separately - fine-dash line the hot NPS, solid line the cool LHB, dash-dot line the GH and broad-dash line the extragalactic power-law continuum. The Al-K line is instrumental (see the background spectrum shown in Fig. 3).

after HWW) have proposed a model of the local cool gas distribution which envisages a local bubble, inside which the cold phase is highly tenuous with $n_H = 0.02$, bounded by an "absorbing wall" at a distance d_w, in which the gas density increases abruptly by a factor ~ 25. Here we use the HWW model to give us an estimate of the extent of the LHB in the direction of the three fields (the values listed under d in Table 2 and under d_w in Table 4).

The extent of Radio Loop I is well approximated by a circle of radius $58° \pm 4°$ with centre at $l_{II} = 329° \pm 1.5°$, $b_{II} = 17.5° \pm 3.0°$ (Berkhuijsen et al. 1971). The distance to the nearest part of Loop I must be > 40 pc, the minimum distance to the edge of the LHB (and the cold ISM wall beyond) and observations of optical starlight polarisation indicate that the distance to the NPS is 100 ± 20 pc (Bingham 1967). It has been suggested by previous authors, e.g. Egger and Aschenbach (1995), that Loop I has interacted with the Local Hot Bubble introducing a flattening of the envelopes of both bubbles. Here we adopted a somewhat different modelling approach. Observationally the bright 0.75 keV X-ray emission from Loop I is confined to the East and South within a circle of radius $\sim 42°$ centred at $l_{II} = 352°$, $b_{II} = 15°$ as shown in Fig. 1. The northern fainter extent of the NPS and some emission in the South West falls outside this circle but the bulk of the emission is contained in this area. We have therefore adopted a spherical volume coincident with this circle as a geometrical model for the X-ray emitting volume, interpreting this feature as a spherical sub-superbubble within Loop I. The circular region also covers 0.75 keV emission from the Galactic Bulge, as discussed in the introduction, and the morphology is complicated by absorption along the Galactic Plane and to the East of centre. However, the appearance of the NPS in the North East, seen in both radio and X-ray emission, is highly suggestive of a limb-brightened shell and it is reasonable to assume that the conditions are fairly uniform along the chords through the shell defined by the lines-of-sight in fields IV, V and VI.

We can calculate the entrance and exit distances along the line of sight, through the Loop I X-ray bubble. Adopting a distance of 210 pc to the centre of the bubble yields a distance to the nearside of the bright parts of the NPS of ~ 100 pc consistent with the polarisation observations. The radius of the bubble is 140 pc and the predicted entrance and exit distances, d_{lo} and d_{hi}, for our particular lines of sight, are given in Table 4. The corresponding distances across the bubble, along the line of sight, are given as d in Table 2. In the absence of any detailed information we adopt an extent of 1 kpc for the GH, beyond the NPS and residual Galactic column. Using these distances and the emission measures from the spectral fits we derived electron densities and pressures for the LHB, NPS and GH components, as shown in Table 1.

The derived temperatures and abundances of the hot (NPS) component are given in Table 3. This table also lists the fraction (F_{N_H}) of the Galactic column applied to the hot component in the spectral modelling (as foreground absorption) and the reduced chi-squared of the fits. The largest contribution to the chi-squared comes from around the Fe XVII and Ne IX lines. This can be best seen in the centre plot of Figure 4, corresponding to Field V. We note that caveats on the use of the APEC code provided on the WWW

Table 2. The emission measures for the three plasma components in fields IV, V and VI. The typical fractional error on the low-temperature components is 8% and on the high temperature component is 4%. d is the adopted line-of-sight distance across the source components used to estimate the electron density and pressure (see text).

		EM cm^{-6} pc	d pc	n_e cm^{-3}	P cm^{-3} K
LHB	IV	0.0040	40	0.011	25600
	V	0.0052	60	0.010	23900
	VI	0.0043	90	0.008	17700
NPS	IV	0.131	164	0.031	180000
	V	0.106	180	0.027	140000
	VI	0.073	134	0.026	142000
GH	IV	0.088	1000	0.010	21900
	V	0.047	1000	0.008	16000
	VI	0.025	1000	0.006	11700

Table 3. Spectral fit parameters for the hot NPS component in fields IV, V and VI. The column labelled F_{N_H} is the fraction of the Galactic N_H which absorbs the hot plasma component. The abundances are with respect to solar values. The last row of the table gives the typical errors on the best-fit values from the spectral fitting.

	χ^2_ν	F_{N_H}	T_{hi} keV	O	Ne	Mg	Fe
IV	1.6	0.9	0.274				
V	2.0	0.6	0.248	0.32	0.44	0.76	0.65
VI	1.0	0.5	0.261				
±		0.1	0.005	0.02	0.04	0.15	0.06

mention discrepancies between the calculated and measured Fe XVII line ratios (see Brown et al. 1998).

6 DISCUSSION

The following sequence of ISM components, along the line of sight towards the NPS, is consistent with the observed MOS spectra and RASS count rates.

- Local Hot Bubble, 40-90 pc
- Cold gas distribution in the wall 15-60 pc
- NPS Superbubble, distance across bubble 130-180 pc
- Residual Galactic column beyond the NPS Superbubble
- Galactic Halo, assumed extent ~ 1000 pc

Table 4. The distance to the wall across the LHB d_w, the distance to the entrance and exit of the NPS bubble d_{lo} and d_{hi}, the column density in front of the NPS emission N_H and the predicted density of the local foreground column in the wall n_H.

	d_w pc	d_{lo} pc	d_{hi} pc	N_H cm^{-2}	n_H cm^{-3}
IV	40	96	260	7.2×10^{20}	4.2
V	60	92	272	3.3×10^{20}	3.3
VI	90	105	239	2.0×10^{20}	4.3

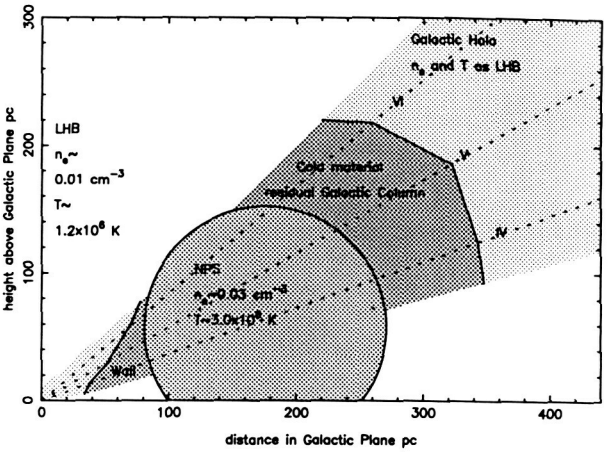

Figure 5. A schematic vertical slice through the Galactic plane at $l_{II} = 20°$ indicating the extent of various hot and cold gaseous components. The lines of sight in fields IV, V and VI are shown as dotted lines.

Fig. 5 shows a schematic vertical slice perpendicular to the Galactic Plane at Galactic longitude 20°.

As mentioned above the distance to the edge of the cavity containing the LHB has been well constrained by ISM absorption line studies which show a rather abrupt and large increase in column density at these distances. The LHB has an hour-glass profile as indicated in Fig. 5. The estimated densities of cold material in the wall between the LHB and NPS given in Table 4 are dependent on the distance to the centre of the bubble and the bubble radius. For radius 140 pc and distance 210 pc the density is ~ 4.0 cm^{-3}. The average density from the onset of the wall out to ~ 400 pc estimated from the all-sky HWW model is 0.4-0.9 cm^{-3} indicating a compression factor in the range 5-11, somewhat lower than the range 20-30 predicted by Yoshioka & Ikeuchi (1990).

The estimated density of ~ 0.028 cm^{-3} within the hot NPS bubble is a factor ~ 10 larger than the average of 0.0025 cm^{-3} quoted by Egger and Aschenbach for this region. This enhancement may be due to the fact that we are viewing tangentially across the brightened limb in the NPS.

Fig. 6 shows a schematic representation of the geometry in a plane angled at 30° to the Galactic Plane. The emission volume we have adopted is offset by ~ 23° (~ 80 pc) from the centre of Loop I (near the centre of mass of the Sco-Cen OB association indicated on Fig. 6) and positioned such that the NPS lies at a distance of ~ 100 pc without having to distort the spherical geometry. Both the present model and that of Egger and Aschenbach (1995) assume that the NPS is a local structure rather than a more distance feature associated with outflow from the Galactic Centre region as suggested by Sofue (2000). The present spectroscopic data, which require that 10-50% of the cold Galactic column lies beyond the NPS emission but in front of the GH component, favour a local interpretation for the NPS.

We have constructed our geometric model to encompass the bulk of the diffuse 0.75 keV emission detected in the RASS. However, some of this emission, in particular that closer to the Galactic plane, may originate in the Galactic Bulge. Detailed analysis of the diffuse SXRB in XMM pointings directed at the Galactic Bulge may shed light on this possibility. It has been conjectured by previous authors (Eg-

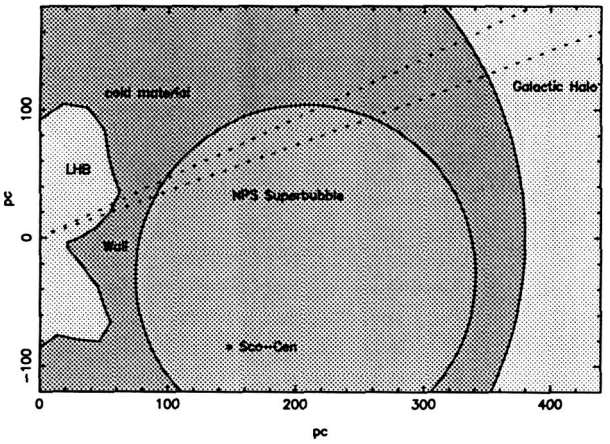

Figure 6. A schematic slice through the Galaxy tilted at an angle of 30° to the Galactic Plane. The straight dotted lines indicate the line-of-sight of the NPS observations. The profile of the LHB is taken from the absorption model of HWW. The Sco-Cen OB association, which is usually taken as the centre of Loop I, is shown at a distance of 170 pc.

ger & Aschenbach and references therein) that the Loop I Superbubble (and the NPS) was produced by outflow from the Scorpio-Centaurus OB association and SNe activity in the same vicinity. If we assume all the observed 0.75 keV emission originates in the NPS superbubble then the total thermal energy in the plasma is at least 10^{51} ergs (using a volume filling factor of 0.1 and the electron pressure given in Table 2). This is consistent with the energy released by a SNe but we might expect a larger filling factor within a single supernova remnant bubble. Given the large offset between the Sco-Cen OB association and the X-ray emission, one or more supernovae events rather than outflow would seem to be the favoured explanation. If the emission corresponds to a single SNR, then the size of the bubble, radius 140 pc, indicates an age of $\sim 2 \times 10^5$ years. For comparison the Vela SNR has a radius of ~ 30 pc and age $\sim 10^4$ years.

The Galactic Halo regions sampled in this study are significantly different from the higher latitude study of KS. The lines of sight are both closer to the Galactic Plane and closer to the Galactic Centre. The high emission measure determined for the GH component may reflect a long path length through the low scale-height KS component. We adopted an effective length of 1000 pc through the GH in Table 2 which yields electron density and pressure estimates that are very similar to the LHB. The conclusion is the same if we assume the halo is a plane parallel distribution with electron density scale height 1000 pc. The observed emission measures of the GH component then correspond to n_e 0.008-0.011 cm^{-3} in the Galactic Plane. There is in fact no absorption wall in directions towards the Galactic Poles (see HWW) and the LHB may not be an isolated bubble but an extension of the Galactic halo in the form of a chimney which extends down to the Galactic Plane in the Solar Neighbourhood (Welsh et al. 1999). If this is the case we may be seeing essentially the same Galactic plasma component at T~0.1 keV both in front of and behind the NPS bubble. Observations with much higher spectral resolution would be required to identify any subtle differences between these two components.

The existence of a GH component at T~0.1 keV has previously been demonstrated unambiguously by shadowing experiments using the ROSAT PSPC, for example Burrows & Mendenhall (1991). The present identification of such a component without shadowing was only possible because of the energy resolution of the MOS detectors and much improved sensitivity in the O VII band 0.5–0.6 keV. In some sense the identification of a GH component in the MOS spectra is only possible due to shadowing by the foreground Galactic column although we are not imaging the edge of a shadow as such. The absorption suppresses the 0.1–0.4 keV signal from the GH component and leaves the O VII line as a prominent feature in the spectrum. The oxygen in the hotter NPS plasma produces a strong O VIII line but contributes very little to the O VII line. We cannot account for the O VII feature by simply increasing the O abundance in the hotter component. Of course, the identification of the absorbed emission from 10^6 K gas as a halo component is based on a single-temperature equilibrium model for the hotter component inside the NPS bubble. This may not be the case since we could be looking at a shock which is still propagating into a steep density gradient. The observed O VII line strength may arise from a range of temperatures and non-equilibrium conditions within the bubble rather than an external halo component further away.

7 CONCLUSION

We have described a robust algorithm for extracting the spectra of the diffuse component of the SXRB from EPIC MOS observations. Analysis of three pointings along the bright ridge of the North Polar Spur provides a quantitative assessment of the components of the local interstellar medium, in this direction, out to a distance of ~ 400 pc. We have been able to measure the temperature and abundances of the NPS plasma with unprecedented accuracy. Comparison of these parameters with the values from similar diffuse components in the Loop I region and the Galactic Bulge will provide a powerful diagnostic tool in the study of this complicated region. The majority of the O VII line feature in the spectrum is attributable to a cool plasma component beyond the Galactic column which we assume is situated in the Galactic Halo.

8 ACKNOWLEDGEMENTS

ADPH acknowledges support from PPARC in the form of a research studentship.

REFERENCES

Bingham, R.C., 1967, MNRAS 137, 157
Berkhuijsen E., Haslam C., Salter C. 1971, Astron. & Atrophys., 14, 252
Brown, G.V., Beiersdorfer, P., Liedahl, D.A., Widmann, K., Kahn, S.M., 1998, Ap.J. 502, 1015
Burrows, D.N. & Mendenhall, J.A, 1991, Nature, 315, 629
Egger R.J. & Aschenbach B. 1995, Astron. & Astrophys. 294, L25
Gendreau K. et al. 1995, Publ. Astron. Soc. Japan, 47, L5
Hutchinson I.B., Warwick R.S., Willngale R. 2003, in preparation

Jahoda K. et al. 1992, in The X-ray Background, ed. X Barcons and A.C. Fabian (Cambridge University Press), 240
Kuntz K.D. & Snowden S.L. 2001, Ap.J. 554, 684
Lumb D.H., Warwick R.S., Page M., De Luca A. 2002, Astron. & Astrophys. 389, 93L
McCammon, D. et al., 2002, Ap.J. 576, 188
Mendenhall, J.A. and Burrows, D.N., 2001, Ap.J. 563, 716
Rocchia R. et al. 1984, Astr. Ap., 130, 53
Sanders W.T. 1993, Proc. SPIE: EUV, X-ray and Gamma-Ray Instrumentation for Astronomy IV, 2006, 221
Sanders, W.T., Edgar, R.J., Kraushaar, W.L., McCammon, D. and Morgenthaler, J.P., 2001, Ap.J. 554, 694
Snowden S.L., Egger R., Finkbeiner D.P., Freyberg M.J., Plucinsky P.P. 1998, Ap. J., 493, 715
Snowden S.L. et al. 1995, Ap. J., 454, 643
Snowden S.L. et al. 1997, Ap. J., 485, 125
Sofue Y. 2000, Ap.J. 540, 224-235
Welsh, B.Y, Sfeir, D.M., Sirk, M.M., Lallement, R, 1999, A&A, 352,308
Yoshioka, S., Ikeuchi, S., 1990, Ap. J. 360, 352